Check for updates

Interesting phase behaviors and ion-conducting properties of dicationic *N*-alkylimidazolium tetrafluoroborate salts†

Hyunho Chae,[a] Yong-Hoon Lee,[a] Minyong Yang,[b] Won-Jin Yoon,[c] Dong Ki Yoon, [bd] Kwang-Un Jeong, [c] Yeon Hwa Song,[e] U Hyek Choi [e] and Minjae Lee [*a]

A series of dicationic imidazolium bis(tetrafluoroborate) salts were newly synthesized, and their phase transition behaviors were correlated with thermal, scattering, optical and conductivity results. The bis-imidazolium salts having side-chain lengths of C_6-C_{10} showed plastic crystal mesophases, while a liquid crystal mesophase was formed in the bis-imidazolium salts with long side-chains (C_{11} and C_{12}). Soft plastic and liquid crystalline phases were also confirmed by wide-angle X-ray diffraction. For the bis-imidazolium salts exhibiting a plastic crystal mesophase, the ionic conductivity suddenly increased at the melting temperature. However, the bis-imidazolium salts with long side-chains showed a slope increase during the liquid crystal-liquid crystal transition.

Introduction

Imidazolium salts have received significant interest because of their wide range of applications as ionic liquids (ILs),[1] organic ionic plastic crystals (OIPCs),[2] and ionic liquid crystals (ILCs).[3] A number of imidazolium salts are commercially available either as room temperature ionic liquids (RTILs) or as ionic salts having higher melting points. The physical and electrical properties of the imidazolium salts have been reported by many scientist groups due to their wide range of applications. Even though numerous imidazolium salts have been synthesized, new imidazolium-based compounds are still being developed, and this kind of study is still worthy to expand the warehouse of ionic materials.

Imidazolium OIPC materials are relatively rare compared to OIPCs of ammonium-based or phosphonium-based ones: a terbium diketonate salt of *N*-(*n*-butyl)-*N*′-methylimidazolium[4] and 1,2-bis[*N*-(*N*′-alkylimidazolium)]ethane salts.[5–8] Some bis-imidazolium salts (Br^- or PF_6^-) showed multiple solid–solid

phase transitions and small ΔS_f values (≤ 12 J K^{-1} mol^{-1}), which corresponded to the classical definition of OIPCs.[9] From solid-state NMR studies, we inferred that the imidazolium rings flip within 30–60 degrees in the soft crystalline phase.[6] Also, a careful observation of ions in the amorphous/crystalline fractions in the solid state by NMR showed that a bis-imidazolium PF_6^- salt with *n*-hexyl side-chains may align in an external magnetic field.[7]

During the last few decades, it has been shown that liquid crystallinity can successfully enhance the ionic conductivity of ionic organic materials.[3,10–13] Due to the nature of long-range ordering in a liquid crystal (LC), a certain bridge, providing high ionic conductivity, is made *via* self-assembly of the molecules. Furthermore, the ionic liquid crystal material is also said to be significantly versatile by means of its self-healing and flexibility. As a result, ionic liquid crystal materials are thought to be future candidates for electrolytes in batteries, solar cells, and fuel cells.[14,15]

Herein, we found that tetrafluoroborate (BF_4^-) salts of dicationic bis-imidazolium compounds also show either OIPC or LC properties. By changing the alkyl side-chain length on the imidazolium moiety, some compounds exhibited plastic crystal phases but others showed liquid crystalline phases. Most of this series of bis-imidazolium salts showed multiple solid–solid phase transitions and small heat absorptions at their melting temperatures. A detailed structure–property relationship of these new imidazolium salts was also discussed.

Results and discussion

The synthetic scheme of the dicationic imidazolium BF_4^- salts is shown in Fig. 1. The bromide salt of 1,2-bis(*N*-alkyl-

Department of Chemistry, Kunsan National University, 558 Daehak-ro, Gunsan, South Korea. E-mail: minjae@kunsan.ac.kr

Graduate School of Nanoscience and Technology, Korean Advanced Institute of Science and Technology, 291 Daehak-ro, Yuseong-gu, Daejeon, South Korea

Department of Polymer-Nano Science and Technology, Chonbuk National University, 567 Baekje-daero, Deokjin-gu, Jeonju, South Korea

Department of Chemistry and KINC, Korean Advanced Institute of Science and Technology, 291 Daehak-ro, Yuseong-gu, Daejeon, South Korea

Department of Polymer Engineering, Pukyong National University, 45 Yongso-ro, Nam-Gu, Busan, South Korea
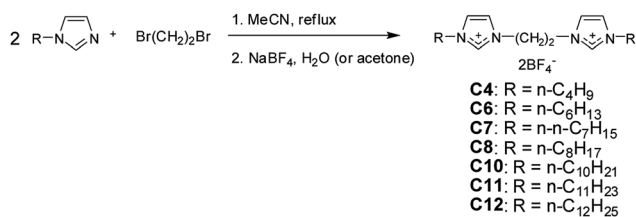
Paper

Fig. 1 Synthesis of a series of 1,2-bis(*N*-alkylimidazolium)ethane BF_4^- salts.
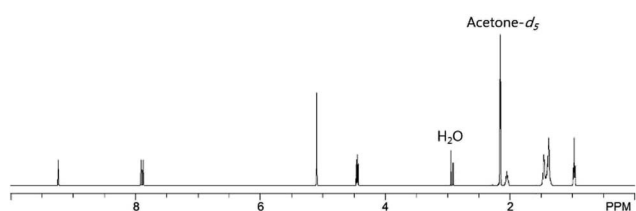

Fig. 2 500 MHz ^{1}H NMR spectrum of **C8** in acetone-d_6.

imidazolium)ethane was prepared first according to a previously reported method.[5,6] Ion exchange reactions were carried out in deionized water or organic solvents, such as acetone or acetonitrile (MeCN). Deionized water was effective in these ion exchange reactions when the BF_4^- salts were insoluble in water; however, organic solvents were used for the water-soluble tetrafluoroborate salts. All the obtained bis-imidazolium BF_4^- salts were negative on the copper-flame test, which showed no remaining bromide anions after anion exchange.

The structures of the synthesized imidazolium BF_4^- salts were confirmed by NMR spectroscopy. In the ^{1}H NMR spectrum (Fig. 2), the imidazolium protons of **C8** are shown at δ 7.77, 7.81 and 9.1; the bridge ethylene protons are present at δ 5.0 (singlet), and the N–CH$_2$ protons can be found at δ 4.3 (triplet), which correspond to previously reported results.[5] The other alkyl protons of the alkyl side-chains are shown at a higher field. The ^{1}H NMR spectra of the other compounds were almost the same except for the integration numbers of the alkyl side-chain peaks.

The thermal stability of the bis-imidazolium BF_4^- salts was confirmed by TGA experiments under an N_2 atmosphere. As shown in Table 1, all the BF_4^- salts were thermally stable up to 310 °C. The thermal decomposition mechanism was mostly 1-step from the 1st derivative line of the TGA thermograms (ESI, Fig. S9†).

The thermal phase behaviors of the synthesized bis-imidazolium BF_4^- salts are summarized in Table 1. Also, the dependence of melting temperature and solid–solid phase transition temperature on the side-chain length of the imidazolium salts is shown in Fig. 3. Phase changes including glass transition temperature (T_g), solid–solid phase transition temperature (T_{ss}) and melting temperature (T_m) of the imidazolium salts were analyzed by differential scanning calorimetry (DSC) and mostly on a second heating scan. Melting temperatures were also visually confirmed by a melting point apparatus. T_m of the dicationic imidazolium BF_4^- salts increased with the increase in the length of the alkyl side-chains from C$_6$ to C$_{10}$; however, the T_m values of **C11** and **C12** were lower than T_m of **C10**. The melting peaks of **C11** and **C12** were quite small due to the small heat absorptions during melting.

From **C6** to **C12**, every bis-imidazolium salt showed one or multiple solid–solid phase transitions during the second heating scan in the DSC analysis. The first solid–solid transition temperature (T_{ss}) of **C7** was the lowest, and among **C6**, **C7** and **C8**, the heat absorption peak at T_{ss} of **C7** was the most distinct; the molar entropy during the solid–solid transition (ΔS_{ss}) at 28 °C was quite large: 103 J K^{-1} mol^{-1}. Despite the large heat absorption at 28 °C (T_{ss}), **C7** still exhibited a large melting peak in the DSC thermogram (Fig. 4).

The entropies of fusion (ΔS_f) of the bis-imidazolium tetrafluoroborate salts could be calculated from the heat absorptions (J g^{-1}) of the melting peaks and sample weights, as shown in Table 1. The ΔS_f values of **C6–C10** were in the range from 32 to 39 J K^{-1} mol^{-1}.

Using a polarized optical microscope (POM), phase sequences of **C6** and **C7** were investigated through the decreasing temperature from their melting phase. Fig. 6a shows the POM image at 100 °C after the first crystallization occurs; here, uniformly aligned crystalline domains as large as a few

Table 1 Thermal properties of the 1,2-bis(*N*-alkylimidazolium)ethane BF_4^- salts

Entry	DSC T_{ss} (°C) [$\sum\Delta S_{ss}{}^a$ (J K^{-1} mol^{-1})]	T_m (°C)	$\Delta S_f{}^b$ (J K^{-1} mol^{-1})	Melting point (°C)	TGA 5% weight loss (°C)
C4	-31^c	81, 246^d	—	79.4–84.0	353
C6	72 [9]	129	38	116.3–119.6	350
C7	28, 75 [103]	158	39	157.1–159.0	356
C8	37, 55 [13]	174	32	173.1–175.3	331
C10	34, 56, 85 [149]	191	33	186.2–191.0	354
C11	66, 75, 82 [133]	180 (LC–LC)	18	178.6–182.2	317
		205 (LC–I)	3.8		
C12	42, 76, 90 [119]	187 (LC–LC)	17	185.5–190.7	321
		254 (LC–I)	3.3		

^{a} $\sum\Delta S_{ss}$ is calculated from the summation of ΔS_{ss} values at all T_{ss} transitions.[16] ^{b} $\Delta S_f = \Delta H_f$ (J mol^{-1})/T (K).[17] ^{c} **C4** showed T_g at -31 °C on the second heating scan. ^{d} Two heat absorption peaks only on the first heating scan but no heat absorption peak on the second heating scan.
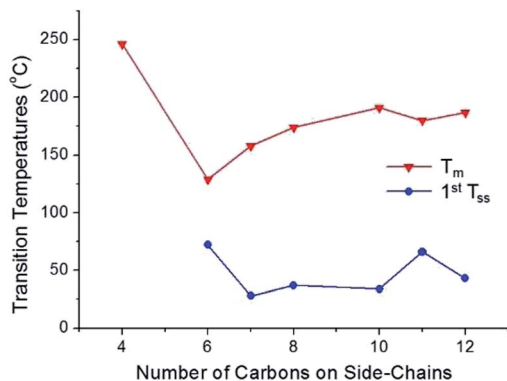
Fig. 3 Relationship between the side-chain length and melting temperature/first solid–solid phase transition temperature for the synthesized dicationic imidazolium BF_4^- salts.

millimeters are observed with strong birefringence. This highly ordered texture was preserved after cooling to room temperature (Fig. 6b) with a cooling rate of 1 °C min^{-1} as the phase transition at 72 °C was suppressed. The only notable change was the elongation of dark domains, possibly made of macro-separated tetrafluoroborates, which were not ordered after the first crystallization. We suggested that the separated anions were elongated through the cationic channel, which was parallel to the direction of the crystal growth.

After the sample was kept at room temperature overnight, suppressed phase transition finally occurred, due to which disordered crystal texture was generated (Fig. 6d). In the case of C7, similar to that observed for C6, uniformly aligned crystalline texture with disordered dark domains was observed immediately after first crystallization (Fig. 6e). After cooling to 100 °C, again, similar to the observation for C6, the dark domains were aligned through the crystalline domain (Fig. 6f). However, the elongated dark domains were significantly thicker than those of C6. When further cooled to 50 °C, undulation perpendicular to the crystal growth direction was generated. Furthermore, when the sample was cooled to room temperature, a domain crack induced by shrinking was generated (Fig. 6g). In this phase, in
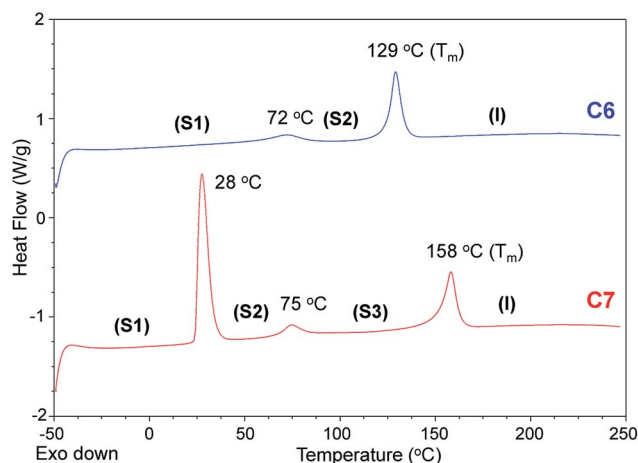

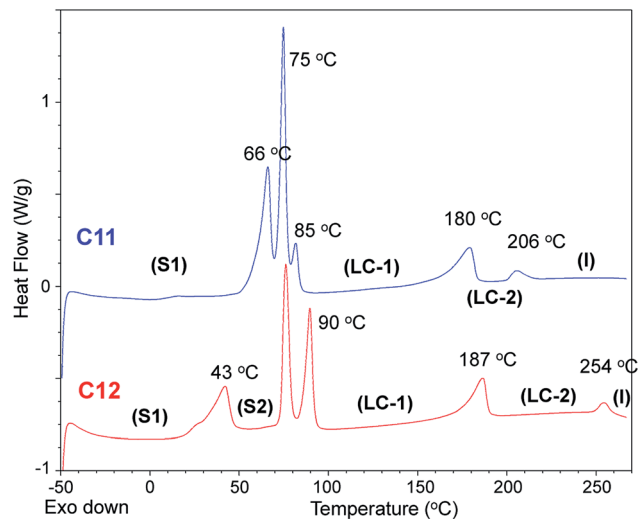Fig. 4 DSC thermograms of C6 (blue) and C7 (red) (2nd heating scans, heating rate = 10 K min^{-1}, N$_2$).

Fig. 5 DSC thermograms of C11 (blue) and C12 (red) (2nd heating scans, heating rate = 10 K min^{-1}, N$_2$). The small T_m peaks of C11 and C12 correspond to the small ΔS_f values: 18 and 17 J K^{-1} mol^{-1}, respectively.

contrast to the observation for C6, the molecular orientation was almost conserved after the last solid–solid phase transition (Fig. 6h). In the case of both C6 and C7, according to the existence of birefringence, it could be noted that the molecules were aligned parallel to the substrate. This alignment could possibly result in an ion-conductive bridge made of the aligned imidazolium moieties.

Bis-imidazolium tetrafluoroborate salts with long alkyl chains, C11 and C12, showed unique phase behaviors compared to other compounds. The ΔS values of C11 and C12 were quite small: 18 and 17 J K^{-1} mol^{-1} for LC–LC phase transitions and 3.8 and 3.3 J K^{-1} mol^{-1} for LC–isotropic transitions, respectively; the total entropy changes at their solid–solid phase transitions were large: 133 and 117 J K^{-1} mol^{-1}, respectively. For C11 and C12, a liquid crystalline phase sequence was observed during both the heating and cooling processes. In particular, within C11 and C12, smectic-like liquid crystalline texture was observed in the POM experiments. During the cooling process, a batonnet-like structure was generated at the melting temperature, which was transformed to a typical smectic fan-shaped structure on further cooling (Fig. 7). The blue and yellow optical domains in the right side of Fig. 7a signify the parallelly and perpendicularly aligned molecular directors with the optic axis (λ) of the full wave plate, respectively.[18,19] From the liquid crystalline texture, similar to the observations for C6 and C7, it was suggested that the C12 molecules in each layer were aligned parallel to the substrate surface, which resulted in the ion-conductive bridge between the two substrates made by the imidazolium moieties of C12.

Also, after the phase transition to the smectic X phase and crystal phase, it can be supposed that this conductive bridge is conserved as the molecular orientation is still parallel to the substrate surface in these phases. As revealed in POM images, the direction of liquid crystalline domains cannot be controlled
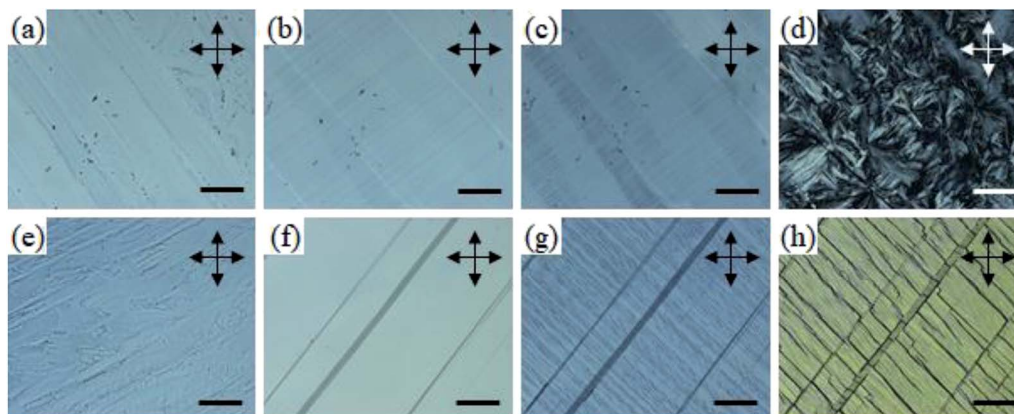
Fig. 6 POM images of (a–d) **C6** and (e–h) **C7** during cooling from their isotropic phases: (a) plastic crystal phase at 100 °C, (b) dark domains aligned at 80 °C before the solid–solid phase transition, (c) plastic crystal phase cooled to room temperature, and (d) crystalline texture after slow crystallization at room temperature. For **C7**: (e) plastic crystal phase at 150 °C, (f) dark domains aligned at 100 °C, (g) undulated pattern in the lower phase at 50 °C, and (h) cracked crystalline texture at room temperature. All scale bars correspond to 200 µm.
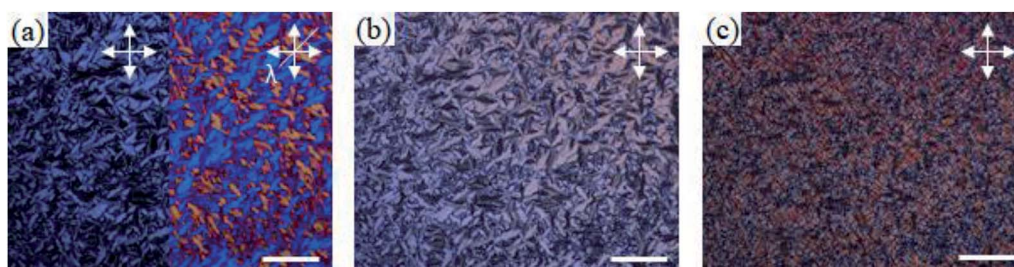

Fig. 7 POM images of **C12** during cooling from its isotropic phase: (a) at 200 °C, (b) at 150 °C, (c) at room temperature. All scale bars correspond to 200 µm.

by a conventional rubbing method similar to the observations for other smectic phases with a direct phase transition from the isotropic phase to the smectic phase.

As shown in Fig. 8, 1D wide-angle X-ray scattering (1D WAXD) patterns are obtained during heating at the rate of 10 °C min^{-1}, corresponding to the POM images of **C7** and **C12** in Fig. 6 and 7. When the temperature was 20 °C, diffraction patterns were detected at $2\theta = 4.8°$ (d-spacing = 1.84 nm) in the
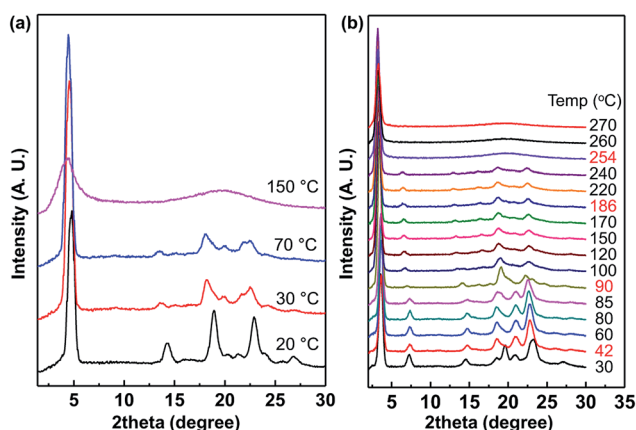

Fig. 8 1D wide-angle X-ray scattering spectra of (a) the plastic crystal **C7** and (b) the liquid crystal **C12** at different temperatures.

low-angle region, 14.3° (d-spacing = 0.62 nm), 18.9–23° from alkyl chain crystal peaks and 25.65° (d-spacing = 0.35 nm) from π–π interaction peaks in the wide-angle region. The diffraction peak at $2\theta = 4.8°$ originated from the layer packing of **C7** molecules. The disappearance of the peak at $2\theta = 25.65°$ over 30 °C showed the loss of the intermolecular π–π interactions between imidazolium rings, which directly corresponded to the plastic crystalline phase (Fig. 6g, 50 °C) and the cracked crystalline phase (Fig. 6(h), 25 °C). Over 150 °C, the diffraction patterns of the wide-angle region changed to a broad amorphous halo with maximum intensity at $2\theta = 19.9°$, while the single diffraction peak in the low-angle region ($2\theta = 4.4°$) remained.

As shown in Fig. 8b, the peak patterns between $2\theta = 18$ and 25° at 30 °C are different from those in the range of 42–85 °C and this corresponds to T_{ss} at 43 °C in the DSC thermogram (Fig. 5). In the spectra from 100 °C to 240 °C, the peak positions are almost the same even though the peak intensities are slightly weakened at higher temperatures. The phase transition at 187 °C of the corresponding DSC curve is not observed in the XRD spectra. Therefore, the LC phase was formed from the crystalline phase after the large heat absorptions, and the LC phase was maintained up to 240 °C. The isotropic phase was also confirmed by XRD above 254 °C, where no significant peak was observed at a value larger than $2\theta = 5°$.
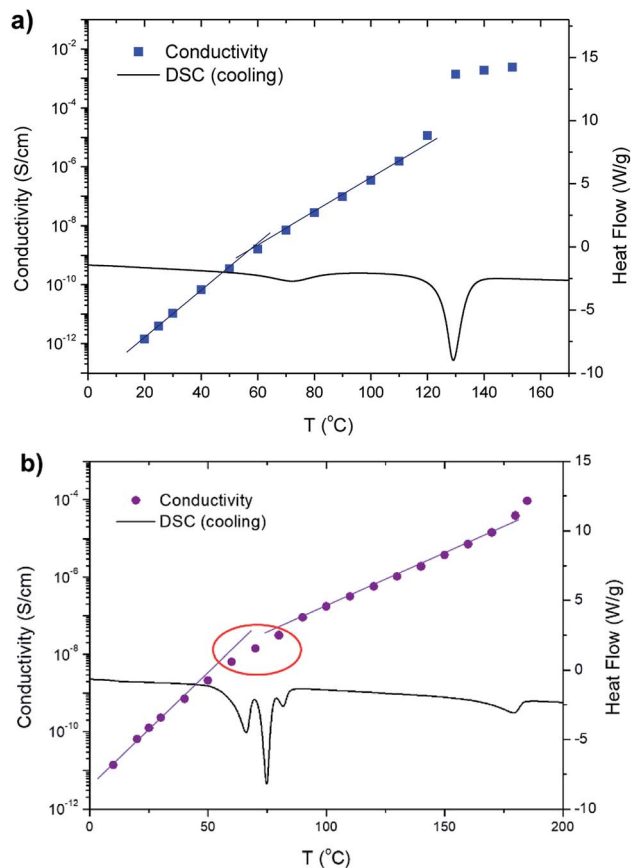
Fig. 9   Ionic conductivity (left axis) as a function of temperature while cooling combined with DSC cooling traces (right axis) for (a) **C6** and (b) **C11**.

Ionic conductivity as a function of temperature while cooling was measured for the bis-imidazolium BF_4^- salts using dielectric relaxation spectroscopy. These salts generally reveal conductivities in the range from 10^{-14} to 10^{-3} S cm^{-1} with discontinuities and changes in slopes at either the solid–solid or melting phase transitions. The results for **C6** and **C11** are exemplarily shown in Fig. 9. For **C6**, the slope changes occurred at around 60 °C, which was slightly below the solid–solid transition temperature (72 °C) detected by DSC; this may be attributed to a slight thermal lag of the cooling chamber of dielectric relaxation spectroscopy (Fig. 9a). Significantly enhanced conductivity over 10^{-3} S cm^{-1} was observed at 130 °C due to the melting transition, i.e., the formation of its isotropic phase, where **C6** becomes a molten salt (similar to an ionic liquid). **C7** showed similar behaviors (ESI, Fig. S15†). At T_{ss} = 28 °C, the conductivity slope change occurred, and a sharp increase was observed during its melting at 158 °C similar to the results for **C6**. As shown in Fig. 9b, **C11** exhibits change in the conductivity slope at 50–80 °C, where both the solid–solid and solid–LC transitions occur (Fig. 5). Above 100 °C, the phase transition from the solid to softer LC phase led to a lower slope in conductivity, presumably indicating decrease in the activation energy of ion conduction. Also, some of the dots of the conductivity plot at 50–80 °C are away from the two trend lines

because multiple phase transitions occur in that temperature range (red circle in Fig. 9b). Furthermore, another conductivity slope change is shown near 170 °C, where the LC1–LC2 phase transition is detected by DSC, POM, and 1D XRD.

Conclusions

New dicationic imidazolium bis(tetrafluoroborate) salts were synthesized and their thermal phase behaviors were studied. The bis-imidazolium BF_4^- salts were stable up to 315 °C, as confirmed by TGA, and their thermal degradations involved a one-step pathway. DSC indicated that **C6** exhibited a single solid–solid phase transition, but **C7–C12** showed multiple heat absorption peaks below their melting temperatures. **C4** showed two melting peaks for the first heating scan but no transition (amorphous) during the second scan. From the POM investigations through decreasing temperature from the isotropic phase, we found that **C6** and **C7** have plastic crystalline phases; uniformly aligned crystalline textures with disordered dark domains were observed and they were maintained until the lowest solid–solid phase transition temperature. For **C11** and **C12** with longer side-chains, POM images showed smectic A fan-shaped liquid crystalline textures. The smectic phase was retained to the lowest phase transition temperature and it turned to a stable crystalline phase. Thus, we found that different lengths of the alkyl side-chains can change the ordering behaviors from plastic crystalline phases with shorter C_6 or C_7 side-chains to liquid crystalline phases with longer C_{11} and C_{12} ones even though all the salts have an identical bis-imidazolium unit. The smaller molar ΔS values of **C11** and **C12** for LC–LC (18 and 17 J K^{-1} mol^{-1}) and LC–isotropic phase transitions (3.8 and 3.3 J K^{-1} mol^{-1}) compared to the larger ΔS_f values of **C6** and **C7** (38 and 38 J K^{-1} mol^{-1}) may be explained by the existence of relatively less ordered liquid crystalline phases of **C11** and **C12**. The wide-angle X-ray scattering results with decreasing temperatures also supported these unique phase behaviors with different chemical structures. The ionic conductivity changes of **C6** showed a large increase at the melting temperature, which can be explained by the transition of long-ordered plastic crystalline to isotropic phase. For **C11**, the less-ordered liquid crystalline smectic A phase showed higher ionic conductivity and the LC–LC phase transition just showed a slope change in the conductivity.

Experimental

Materials

N-Alkylimidazoles were prepared following previously reported procedures.[5,6] Acetone as a reaction solvent was dried over anhydrous $CaSO_4$ and then distilled. Acetonitrile (MeCN) as a reaction solvent was dried over anhydrous K_2CO_3 and then distilled. Tetrahydrofuran (THF) was distilled with some benzoquinone and sodium. Deuterated NMR solvents were bought from Cambridge Isotope Laboratories and used as received. All other chemicals and solvents were used as received.

Instruments

^{1}H and ^{13}C NMR spectra were obtained on a Varian VNMRS 500 MHz spectrometer. The molecular mass values of the compounds were analyzed by a Synapt G2 HDMS quadrupole time-of-flight (TOF) mass spectrometer equipped with an electrospray ion source (Waters, Milford, MA, USA) in positive ion mode. DSC results were obtained on a TA Instrument Q200 differential scanning calorimeter with a scan rate of 10 K min^{-1} under N$_2$. TGA results were obtained on a TA Instrument SDT Q600 Simultaneous TGA/DSC with a heating rate of 10 K min^{-1} under N$_2$. Melting points were observed on an Electrothermal 9300 melting point apparatus with a 1 K min^{-1} heating rate. Ionic conductivity was measured on a Novocontrol GmbH Concept 40 broad band dielectric spectrometer. Samples for dielectric relaxation spectroscopic measurements were placed on a 30 mm-diameter polished brass electrode and dried *in vacuo* at 100 °C for 24 h, after which a second polished brass electrode with 15 mm diameter was placed on top of the sample. Also, 50 μm silica-rod spacers were used to control the sample thickness. Data were collected in isothermal frequency sweeps every 5 K from 220 to 0 °C under a dry N$_2$ flow. Frequency sweeps were performed isothermally from 10 MHz to 0.01 Hz for every measurement.

Polarized optical microscope

Direct visualization of optical textures was carried out by POM (LV100POL, Nikon) equipped with a charge-coupled device (CCD) camera (DS-Ri1, Nikon). The temperature was controlled with the heating stage (Linkam LTS420) and a temperature controller (Linkam TMS94).

Wide-angle X-ray diffraction

The 1D WAXD patterns were obtained by using D8 Discover 3 kW, Bruker AXS. The diffraction peak positions and widths were calibrated with silver behenate in the low-angle region and a silicon crystal standard in the wide-angle region. To monitor the phase transition with temperature changes, a hot stage was calibrated to be ±1 °C error. Samples were scanned across a 2θ-angle range from 2° to 30°.

Synthetic procedures for bis-imidazolium BF$_4$$^{-}$ salts

1,2-Bis[N-(N′-butylimidazolium)]ethane 2BF$_4$$^{-}$ (C4). A solution of 1-butylimidazole (0.999 g, 8.0 mmol) and 1,2-dibromoethane (0.756 g, 4.0 mmol) in MeCN (20 mL) was refluxed for 3 days. After cooling to room temperature, the precipitate was filtered and washed with THF three times. Drying in a vacuum oven gave a colorless crystalline bromide salt (1.41 g, 63%). A solution of the bromide salt (0.219 g, 0.5 mmol) and NaBF$_4$ (0.116 g, 1.05 mmol) in anhydrous acetone (2 mL) was stirred for 24 hours at ambient temperature. The precipitate was filtered and dried in a vacuum oven to obtain a colorless crystalline solid **C4** (0.222 g, 94% from the bromide salt). Mp 79–84 °C. ^{1}H NMR (500 MHz, acetone-d_6, 23 °C): δ 0.93 (t, J = 8, 6H), 1.35 (m, 4H), 1.91 (m, 4H), 4.34 (t, J = 8, 4H), 4.97 (s, 4H), 7.75 (t, J = 1.5,

2H), 7.79 (t, J = 1.5, 2H), 9.07 (s, 2H). ^{13}C NMR (125 MHz, acetone-d_6, 23 °C): δ 13, 20, 32, 49, 50, 123, 124, 137.

1,2-Bis[N-(N′-hexylimidazolium)]ethane 2BF$_4$$^{-}$ (C6). A solution of 1-hexylimidazole (3.35 g, 22 mmol) and 1,2-dibromoethane (2.07 g, 11 mmol) in MeCN (20 mL) was refluxed for 3 days. After cooling to room temperature, the precipitate was filtered and washed with THF three times. Drying in a vacuum oven gave a colorless crystalline bromide salt (3.39 g, 63%). A solution of the bromide salt (0.985 g, 2.0 mmol) and NaBF$_4$ (4 equiv.) in deionized water (5 mL) was stirred for 24 hours at ambient temperature. The precipitate was filtered and dried in a vacuum oven to obtain a colorless crystalline solid **C6** (0.954 g, 86% from the bromide salt). Mp 116–119 °C. ^{1}H NMR (500 MHz, acetone-d_6, 23 °C): δ 0.86 (t, J = 8, 6H), 1.32 (m, 12H), 1.93 (m, 4H), 4.34 (t, J = 8, 4H), 4.98 (s, 4H), 7.75 (t, J = 1.5, 2H), 7.82 (t, J = 1.5, 2H), 9.04 (s, 2H). ^{13}C NMR (125 MHz, acetone-d_6, 22 °C): δ 14, 22, 26, 30, 31, 49, 50, 123, 124, 137.

1,2-Bis[N-(N′-heptylimidazolium)]ethane 2BF$_4$$^{-}$ (C7). A solution of 1-heptylimidazole (3.66 g, 22 mmol) and 1,2-dibromoethane (2.07 g, 11 mmol) in MeCN (20 mL) was refluxed for 3 days. After cooling to room temperature, the precipitate was filtered and washed with THF three times. Drying in a vacuum oven gave a colorless crystalline bromide salt (3.88 g, 68%). A solution of the bromide salt (1.04 g, 2.0 mmol) and NaBF$_4$ (4 equiv.) in deionized water (5 mL) was stirred for 24 hours at ambient temperature. The precipitate was filtered and dried in a vacuum oven to obtain a colorless crystalline solid **C7** (0.959 g, 83% from the bromide salt). Mp 157–159 °C. ^{1}H NMR (500 MHz, acetone-d_6, 23 °C): δ 0.86 (t, J = 8, 6H), 1.27–1.34 (m, 16H), 1.93 (m, 4H), 4.33 (t, J = 8, 4H), 4.96 (s, 4H), 7.73 (t, J = 1.5, 2H), 7.80 (t, J = 1.5, 2H), 9.02 (s, 2H). ^{13}C NMR (125 MHz, acetone-d_6, 23 °C): δ 14, 23, 27, 29, 31, 32, 50, 51, 123.9, 124.1, 138. HRMS (ESI): m/z 447.3281 ([M − BF$_4$]$^{+}$ (calcd for C$_{22}$H$_{40}$N$_4$BF$_4$ 447.3282, error 0.2 ppm)).

1,2-Bis[N-(N′-octylimidazolium)]ethane 2BF$_4$$^{-}$ (C8). A solution of 1-octylimidazole (5.05 g, 28 mmol) and 1,2-dibromoethane (2.63 g, 14 mmol) in MeCN (20 mL) was refluxed for 3 days. After cooling to room temperature, the precipitate was filtered and washed with THF three times. Drying in a vacuum oven gave a colorless crystalline bromide salt (5.86 g, 76%). A solution of the bromide salt (0.980 g, 1.8 mmol) and NaBF$_4$ (4 equiv.) in deionized water was stirred for 24 hours at ambient temperature. The precipitate was filtered and dried in a vacuum oven to obtain a colorless crystalline solid **C8** (0.962 g, 89% from the bromide salt). Mp 173–175 °C. ^{1}H NMR (500 MHz, acetone-d_6, 23 °C): δ 0.86 (t, J = 8, 6H), 1.28–1.36 (m, 20H), 1.95 (m, 4H), 4.34 (t, J = 8, 4H), 4.99 (s, 4H), 7.77 (t, J = 1.5, 2H), 7.80 (t, J = 1.5, 2H), 9.13 (s, 2H). ^{13}C NMR (125 MHz, acetone-d_6, 23 °C): δ 14, 24, 27, 29.6, 29.7, 30, 32, 50, 51, 123, 124, 137.

1,2-Bis[N-(N′-decylimidazolium)]ethane 2BF$_4$$^{-}$ (C10). A solution of 1-decylimidazole (4.58 g, 22 mmol) and 1,2-dibromoethane (2.07 g, 11 mmol) in MeCN (20 mL) was refluxed for 3 days. After cooling to room temperature, the precipitate was filtered and washed with THF three times. Drying in a vacuum oven gave a colorless crystalline bromide salt (5.17 g, 79%). A solution of the bromide salt (1.21 g, 2.0 mmol) and NaBF$_4$ (4 equiv.) in deionized water was stirred for 24 hours at ambient

temperature. The precipitate was filtered and dried in a vacuum oven to obtain a colorless crystalline solid C10 (1.23 g, 93% from the bromide salt). Mp 186–191 °C. ^{1}H NMR (500 MHz, acetone-d_6, 23 °C): δ 0.86 (t, $J = 8$, 6H), 1.28–1.36 (m, 28H), 1.95 (m, 4H), 4.34 (t, $J = 8$, 4H), 4.98 (s, 4H), 7.75 (t, $J = 1.5$, 2H), 7.82 (t, $J = 1.5$, 2H), 9.03 (s, 2H). ^{13}C NMR (125 MHz, acetone-d_6, 23 °C): δ 14, 24, 27, 29.8, 30.0, 30.1, 30.3, 30.7, 31, 33, 50, 51, 124, 124, 138.

1,2-Bis[N-(N′-undecylimidazolium)]ethane 2BF$_4$$^-$ (C11). A solution of 1-undecylimidazole (8.89 g, 40 mmol) and 1,2-dibromoethane (3.76 g, 20 mmol) in MeCN (40 mL) was refluxed for 3 days. After cooling to room temperature, the precipitate was filtered and washed with THF three times. Drying in a vacuum oven gave a colorless crystalline bromide salt (9.66 g, 76%). A solution of the bromide salt (0.978 g, 1.5 mmol) and NaBF$_4$ (4 equiv.) in deionized water was stirred for 24 hours at ambient temperature. The precipitate was filtered and dried in a vacuum oven to obtain a colorless crystalline solid C11 (1.00 g, 94% from the bromide salt). Mp 178–182 °C. ^{1}H NMR (500 MHz, acetone-d_6, 23 °C): δ 0.86 (t, $J = 8$, 6H), 1.27–1.35 (m, 32H), 1.94 (m, 4H), 4.34 (t, $J = 8$, 4H), 5.00 (s, 4H), 7.78 (t, $J = 1.5$, 2H), 7.80 (t, $J = 1.5$, 2H), 9.18 (s, 2H). ^{13}C NMR (125 MHz, acetone-d_6, 23 °C): δ 14, 23, 27, 29.8, 30.1, 30.2, 30.3, 30.4, 30.7, 33, 50, 51, 123.9, 124.0, 138.

1,2-Bis[N-(N′-dodecylimidazolium)]ethane 2BF$_4$$^-$ (C12). A solution of 1-dodecylimidazole (9.45 g, 40 mmol) and 1,2-dibromoethane (3.76 g, 20 mmol) in MeCN (40 mL) was refluxed for 3 days. After cooling to room temperature, the precipitate was filtered and washed with THF three times. Drying in a vacuum oven gave a colorless crystalline bromide salt (9.99 g, 76%). A solution of the bromide salt (0.999 g, 1.5 mmol) and NaBF$_4$ (4 equiv.) in deionized water was stirred for 24 hours at ambient temperature. The precipitate was filtered and dried in a vacuum oven to obtain a colorless crystalline solid C12 (0.991 g, 91% from the bromide salt). Mp 178–182 °C. ^{1}H NMR (500 MHz, acetone-d_6, 23 °C): δ 0.87 (t, $J = 8$, 6H), 1.28–1.36 (m, 36H), 1.95 (m, 4H), 4.34 (t, $J = 8$, 4H), 4.99 (s, 4H), 7.77 (t, $J = 1.5$, 2H), 7.81 (t, $J = 1.5$, 2H), 9.12 (s, 2H). ^{13}C NMR (125 MHz, acetone-d_6, 23 °C): δ 14, 23, 27, 29.8, 30.0, 30.1, 31.3, 31.42, 31.44, 30.6, 33, 50, 51, 123.8, 124.0, 138. HRMS (ESI): m/z 587.4809 ([M − BF$_4$]$^+$ (calcd for C$_{32}$H$_{60}$N$_4$BF$_4$ 587.4847, error 6.5 ppm)).

Conflicts of interest

There are no conflicts to declare.

Acknowledgements

Notes and references

1 Recent review papers: (a) S. Wang and X. Wang, Angew. Chem., Int. Ed., 2016, 55, 2308–2320; (b) B. Wang, Q. Li, T. Mu, Z. Xue and G. Gao, Chem. Rev., 2017, 117, 7113–7131; (c) K. Dong, S. Zhang and J. Wang, Chem. Commun., 2016, 52, 6744–6764.

2 Recent review papers: (a) M. Forsyth, F. Chen, L. A. O'Dell and K. Romanenko, Solid State Ionics, 2016, 288, 160–166; (b) J. M. Pringle, J. Adebahr, D. R. MacFarlane and M. Forsyth, Phys. Chem. Chem. Phys., 2010, 12, 7234.

3 Recent review papers: (a) A. A. Fernandez and P. H. J. Kouwer, Int. J. Mol. Sci., 2016, 17, 731; (b) K. Goossens, K. Lava, C. W. Bielawski and K. Binnemans, Chem. Rev., 2016, 116, 4643–4807.

4 S.-F. Tang and A.-V. Mudring, Eur. J. Inorg. Chem., 2009, 19, 2769.

5 M. Lee, Z. Niu, C. Slebodnick and H. W. Gibson, J. Phys. Chem. B, 2010, 114, 7312–7319.

6 M. Lee, U. H. Choi, S. Wi, C. Slebodnick, R. H. Colby and H. W. Gibson, J. Mater. Chem., 2011, 21, 12280–12287.

7 B. E. Kidd, M. D. Lingwood, M. Lee, H. W. Gibson and L. A. Madsen, J. Phys. Chem. B, 2014, 118, 2176–2185.

8 M. Lee, Y.-H. Lee, J. H. Park and U. H. Choi, Org. Electron., 2017, 48, 241–247.

9 J. Timmermans, Phys. Chem. Solids, 1961, 18, 1.

10 J. Sakuda, M. Yoshio, T. Ichikawa, H. Ohno and T. Kato, New J. Chem., 2015, 39, 4471–4477.

11 T. Kato, Angew. Chem., Int. Ed., 2010, 49, 7847–7848.

12 Y. Iinuma, K. Kishimoto, Y. Sagara, M. Yoshio, T. Mukai, I. Kobayashi, H. Ohno and T. Kato, Macromolecules, 2007, 40, 4874–4878.

13 M. Yoshio, T. Mukai, K. Kanie, M. Yoshizawa, H. Ohno and T. Kato, Adv. Mater., 2002, 14, 351–354.

14 J. Sakuda, E. Hosono, M. Yoshio, T. Ichikawa, T. Matsumoto, H. Ohno, H. Zhou and T. Kato, Adv. Funct. Mater., 2015, 25, 1206–1212.

15 D. Högberg, B. Soberats, R. Yatagai, S. Uchida, M. Yoshio, L. Kloo, H. Segawa and T. Kato, Chem. Mater., 2016, 28, 6493–6500.

16 The entropy change at solid–solid phase transitions are calculated by the summation of the molar entropies of all heat absorption peaks at T_{ss}. For example, total ΔS_{ss} of C12 was calculated by the summation of each ΔS_{ss} value from the heat absorptions at 43, 76 and 90 °C.

17 ΔS_f and ΔS_{ss} can be calculated from ΔH (J mol^{-1})/T (K). Each ΔH (J mol^{-1}) can be calculated from the heat absorption values (J g^{-1}) from the linear integration of the each T_m (or T_{ss}) peak on DSC and molecular weight of the salts.

18 M.-J. Gim, D. A. Beller and D. K. Yoon, Nat. Commun., 2017, 8, 15453.

19 M.-J. Gim and D. K. Yoon, ACS Appl. Mater. Interfaces, 2016, 8, 27942–27948.